Table 3. Electrophysiological Findings of Four Japanese Patients with KCNV2-retionpathy

Pt	DA 0.01		DA 30.0				Square shaped a-wave	Excessive enlargement of b-wave in the extended protocol	LA 3.0			LA 3.0 30Hz		
			A-wave		B-wave				A-wave	B-wave		B-wave		
	Amp (μv)	PT (ms)	Amp	PT	Amp	PT			Amp	PT	Amp	PT	Amp	PT
1	N	Del	N	Del	Super N	NA	(+)	(+)	Sub N	Del	Sub N	UD	UD	UD
2	UD	UD	N	Del	Super N	NA	(+)	NA	Sub N	Del	Sub N	Del	Sub N	Del
3	Sub N	Del	N	Del	Super N	N	(+)	NA	Sub N	Del	Sub N	Del	Sub N	N
4	Sub N	Del	N	Del	Super N	NA	(+)	(+)	Sub N	Del	Sub N	Del	Sub N	Del

Pt = patient; Amp = amplitude; PT = peak time; N = normal; UD = undetectable response; Sub N = subnormal; Del = delayed response; Super N=supernormal response; NA = not available. Full-field electroretinography (ERG) incorporating the standards of the International Society for Clinical Electrophysiology of Vision (ISCEV) included: (i) dark adapted dim flash 0.01 cd•s•m^{-2} (DA0.01), (ii) dark adapted bright flash 30.0 cd•s•m^{-2} (DA30.0), (iii) light adapted 3.0 cd•s•m^{-2} at 2 Hz (LA 3.0), and (iv) light adapted 3.0 cd•s•m^{-2} 30 Hz flicker (LA 3.0 30 Hz). The extended protocol also included the recording of dark adapted responses to an intensity series of flashes in order to detect an excessive enlargement of dark adapted b-wave (patients 1 and 4).

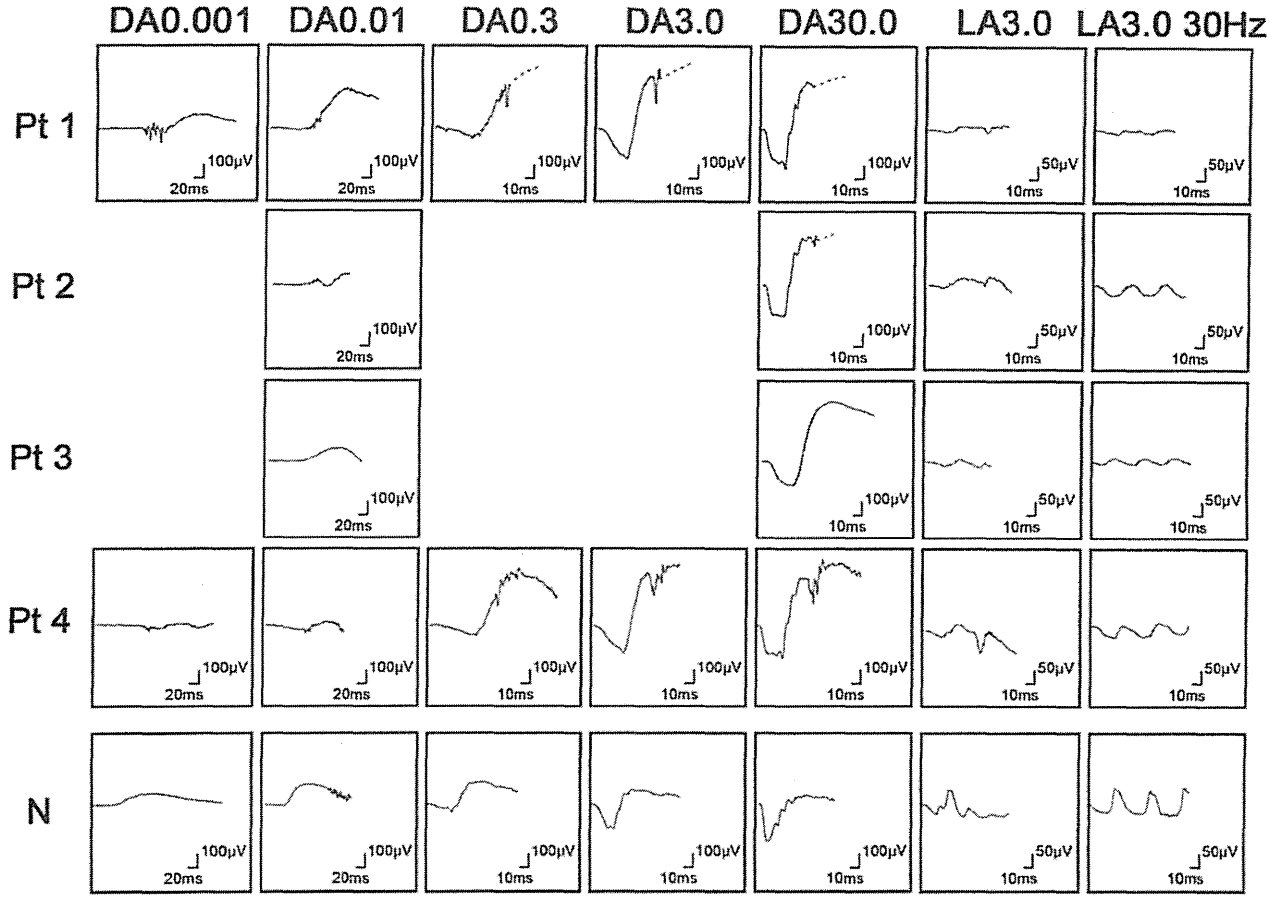

Figure 2. Electrophysiological findings of each patient with potassium channel, subfamily V, member 2 (*KCNV2*) retinopathy. Full-field electroretinograms (ERGs) of patient 1 (top row), patient 2 (second row), patient 3 (third row), and patient 4 (forth row) are shown. The ERGs from a normal control (bottom row) are also shown for comparison. All four patients underwent full-field ERG testing with the minimum standards of the International Society for Clinical Electrophysiology of Vision (ISCEV): (i) dark adapted dim flash 0.01 cd•s•m^{-2} (DA 0.01), (ii) dark adapted bright flash 30.0 cd•s•m^{-2} (DA 30.0), (iii) light adapted 3.0 cd•s•m^{-2} at 2 Hz (LA 3.0), and (iv) light adapted 3.0 cd•s•m^{-2} 30 Hz flicker ERG (LA 3.0 30Hz). The extended protocol was applied to two subjects (patients 1 and 4), including the recording of dark-adapted ERGs to an intensity series of flashes; 0.001 cd•s•m-^{2}, 0.01 cd•s•m^{-2}, 0.3 cd•s•m^{-2}, 3.0 cd•s•m^{-2}, and 30.0 cd•s•m^{-2}.

p.Arg206Pro, were not identified. Three missense variants, p.Arg27His, p.Cys177Arg, and p.Arg206Pro, were highly conserved among the orthologs, and one missense variant, p.Gly461Arg, was completely conserved (Figure 3).

A model of the *KCNV2* protein structure showing the approximate position of the missense disease-causing variants identified is presented in Figure 4. The KCNV2 protein comprises 545 amino acids and contains an N-terminal A and B box (NAB) and six transmembrane domains, (S1–S6), with a K selective motif, GlyTyrGly, in the pore-forming loop (P loop) between S5 and S6 [18]. One variant is located within the N-terminus (p.Arg27His), two variants, p.Cys177Arg and p.Arg206Pro, within the NAB, and one variant, p.Gly461Arg, within the P-loop.

Detailed molecular results of two non-disease-causing variants (polymorphisms) including the in silico analyses are summarized in Appendix 2. These two homozygous variants, p.Gly61Gly and p.Ala265Ala, were synonymous changes in the cording region and were predicted to be benign or have no effect on splicing (Polyphen2 and Human Splicing finder program analysis). Both were present in a high number of chromosomes in the Exome Variant Server database (7647/13006 for p.Gly61Gly and 5636/13006 for p.Ala265Ala, respectively).

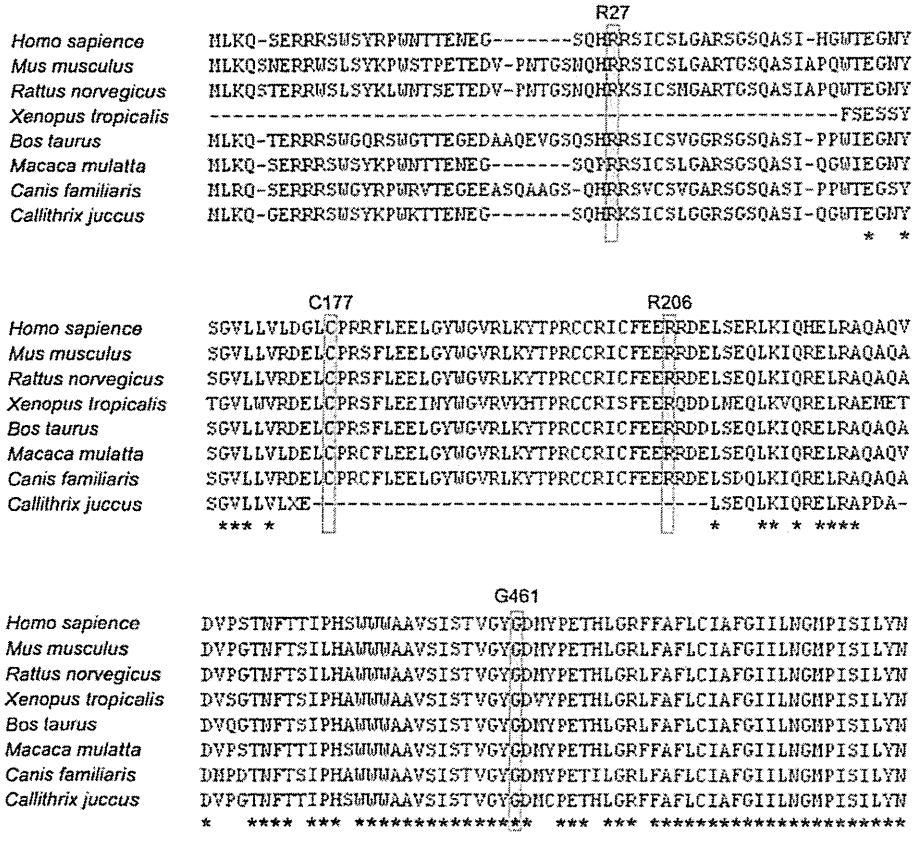

Figure 3. Multiple alignment of eight species of potassium channel, subfamily V, member 2 orthologs. The amino acid-sequence alignment is numbered in accordance with the *Homo sapiens* potassium channel, subfamily V, member 2 (*KCNV2*) sequence (ENSP00000371514). The positions of mutated residues, Arg27 (c.80 G>A, p.Arg27His), Arg177 (c.529 T>C, p.Cys177Arg), Arg206 (c.617 G>C, p.Arg206Pro), and Gly461 (c.1381 G>A, p.Gly461Arg), are highlighted. The alignment was performed with the Clustal Omega program, and the asterisk indicates a completely conserved residue.

DISCUSSION

Our results showed the molecular genetic characteristics of four Japanese patients with CDSRR, which, to the best of our knowledge, is the first report of these characteristics of *KCNV2* retinopathy in an East Asian population. Our four patients harbored the likely disease-causing variants in *KCNV2*. Compound heterozygosity for two alleles, p.Cys177Arg and p.Gly461Arg, in three patients and homozygosity for two complex alleles, p.Arg27His and p.Arg206Pro, in one subject were confirmed. Three of the four variants, p.Arg27His, p.Cys177Arg, and p.Arg206Pro, were novel, which indicates all genotypes identified in our series have never been described before.

The clinical and electrophysiological characteristics of our four patients were similar to those of reported patients [8-11,13,14,17,18]. Additionally, all four patients presented with a decrease in central vision whose onset was in the first decade of life with minimal fundus changes and a characteristic ring enhancement of the AF signal (Table 2 and Figure 1). These findings are also in accordance with earlier reports [9-12,14]. SD-OCT demonstrated a discontinuous or absent inner and outer segment junction line in two patients

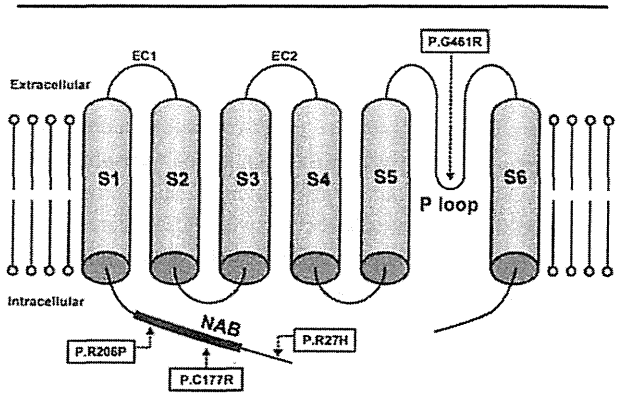

Figure 4. Model of the potassium channel, subfamily V, member 2 protein structure. A schematic representation of the potassium channel, subfamily V, member 2 (*KCNV2*) subunit of the K channel is drawn showing the approximate position of missense disease-causing variants identified in this study. The *KCNV2* protein consists of an N-terminus, an N-terminal A and B box (NAB), and six transmembrane domains (S1–S6), with two extracellular loops (EC 1, 2) and a K selective motif, GlyTyrGly, in the pore-forming loop (P loop) between S5 and S6.

as previously reported [10]. In addition, the absence of the cone outer segment tip line at the macular region was also confirmed in all four patients.

The pathognomonic electrophysiological features were demonstrated in all four patients, viz., delayed and reduced photopic ERGs, delayed ERGs for DA 0.01, and a square-shaped a-wave with a supernormal b-wave for DA 30.0 (Table 3 and Figure 2). An excessive increase in the b-wave for the DA ERGs to an intensity series of flashes was also confirmed in patients 2 and 3. Therefore, the unique rod system abnormalities were identical to those reported for *KCNV2* retinopathy [9,14].

Compound heterozygosity for two alleles, p.Cys177Arg and p.Gly461Arg, was found in patients 1, 2, and 3. The p.Gly461Arg with relatively higher allele frequency affects the third residue of the ultraconserved-GYG-tripeptide motif that acts as an ion selectivity filter in the K channel's pore-forming loop, P loop, between S5 and S6 (Figure 4) [30]. The clinical effect of p.Gly461Arg was well characterized earlier [10,16,17]. Friedburg et al. reported that three siblings with homozygous p.Gly461Arg had a relatively severe phenotype with an early onset and nystagmus at <5 years of age, visual acuity decrease (0.1–0.25, constantly), minimal fundus changes, ring enhancement at the foveal AF image, and an excessive increase in the b-wave for scotopic ERGs to an intensity series [17]. In contrast to the previous reports on homozygous patients, the three patients with heterozygous p.Gly461Arg in our series did not have nystagmus, and two of our patients had less severe BCVA decrease (0.7–0.8). These findings imply that the phenotype of the compound heterozygous for p.Gly461Arg and p Cys177Arg could have a less severe phenotype than those homozygous for p.Gly461Arg. It is of interest that the phenotypic spectrum, compound heterozygous for p.Gly461Arg and p Cys177Arg, was also observed in our series. Two relatively mild phenotypes were observed in the two siblings in our series (patients 1 and 2). In addition, one relatively severe phenotype, with more severe visual acuity decrease (0.1) and photoreceptor/RPE abnormalities at the macula, was detected in patient 3.

Three of the new disease-causing missense variants were located within the N-terminal region of the protein (Figure 4): p.Arg27His within the N-terminus and p.Cys177Arg and p.Arg206Pro within NAB. p.Cys177Arg was completely segregated, and the predicted pathogenesis and evolutionary conservation were confirmed. The coexistence of two likely disease-causing variants, p.Arg27His and p.Arg206Pro, on the same chromosome was also identified in our series with segregation analyses. The patient who was homozygous for these two complex variants had a severe phenotype, with an early onset (2 years), nystagmus, and severe visual acuity decrease (0.1 to 0.08). Both variants were predicted to be pathogenic with evolutionary high conservation (Appendix 1and Figure 3). Whether one of these variants is a neutral polymorphisms in cis with disease-causing one, or whether family 4's alleles are complex with two independently damaging missense variants remains to be determined.

To conclude, this study further delineates the molecular genetic findings of *KCNV2* retinopathy. Three putative novel variants were identified in our four Japanese patients with CDSRR, and our findings suggest there may be a distinct spectrum of *KCNV2* alleles in the Japanese population. However, the clinical findings were similar to that of the reported other population. Electrophysiology was fundamental to the diagnosis with pathognomonic findings due to channelopathy. The pathognomonic characteristics may be a useful method of determining the success of clinical therapeutic trials with gene replacement or pharmacological treatments for channelopathy.

APPENDIX 1. RESULTS OF IN SILICO MOLECULAR GENETIC ANALYSIS OF *KCNV2* MUTATIONS IDENTIFIED.

To access the data, click or select the words "Appendix 1." Pt = patient; Hom = homozygous; Het = heterozygous; SIFT = sorting Intolerant from Tolerance; HSF = human splicing finder program; CV = consensus values; EVS = exome variant server; POD = possibly damaging; PRD = probably damaging; ND = not detected. SIFT (version 4.0.4) results are reported to be tolerant if tolerance index ≥ 0.05 or intolerant if tolerance index < 0.05. Polyphen-2 (vision 2.1) appraises mutations qualitatively as Benign, Possibly Damaging or Probably Damaging based on the model's false positive rate. The cDNA is numbered according to Ensemble transcript ID ENST00000382082, in which +1 is the A of the translation start codon. Human splicing finder version 2.4.1 was applied to predict the effect of each variant on splicing. The results from HSF matrix indicate the values for the wild type and mutant sequences. The larger difference of values between the wild type and the mutant sequences indicates the greater change that the variant can affect on the splice site. EVS denotes variants in the Exome Variant Server, NHLBI Exome Sequencing Project, Seattle, WA.

APPENDIX 2. MOLECULAR ANALYSIS OF *KCNV2* POLYMORPHISMS.

To access the data, click or select the words "Appendix 2." Pt = patient; Hom = homozygous; Het = heterozygous; SIFT = sorting Intolerant from Tolerance; HSF = human splicing

finder program; CV = consensus values; EVS = exome variant server.

ACKNOWLEDGMENTS

We are grateful to the patients who kindly agreed to take part in this study and colleagues who referred individuals to us at National Institute of Sensory Organs. We thank Professor Duco I. Hamasaki (Bascom Palmer Eye Institute, Miami, FL) for proofreading. This research is supported in part by research grants from the Ministry of Health, Labor and Welfare, Japan and Grant-in-Aid for Scientific Research from JSPS.

REFERENCES

1. Gouras P, Eggers HM, MacKay CJ. Cone dystrophy, nyctalopia, and supernormal rod responses. A new retinal degeneration. Arch Ophthalmol 1983; 101:718-24. [PMID: 6601944].
2. Alexander KR, Fishman GA. Supernormal scotopic ERG in cone dystrophy. Br J Ophthalmol 1984; 68:69-78. [PMID: 6607068].
3. Yagasaki K, Miyake Y, Litao RE, Ichikawa K. Two cases of retinal degeneration with an unusual form of electroretinogram. Doc Ophthalmol 1986; 63:73-82. [PMID: 3015524].
4. Foerster MH, Kellner U, Wessing A. Cone dystrophy and supernormal dark-adapted b-waves in the electroretinogram. Graefes Arch Clin Exp Ophthalmol 1990; 228:116-9. [PMID: 2186970].
5. Kato M, Kobayashi R, Watanabe I. Cone dysfunction and supernormal scotopic electroretinogram with a high-intensity stimulus. A report of three cases. Doc Ophthalmol 1993; 84:71-81. [PMID: 8223112].
6. Rosenberg T, Simonsen SE. Retinal cone dysfunction of supernormal rod ERG type. Five new cases. Acta Ophthalmol (Copenh) 1993; 71:246-55. [PMID: 8333273].
7. Hood DC, Cideciyan AV, Halevy DA, Jacobson SG. Sites of disease action in a retinal dystrophy with supernormal and delayed rod electroretinogram b-waves. Vision Res 1996; 36:889-901. [PMID: 8736222].
8. Michaelides M, Holder GE, Webster AR, Hunt DM, Bird AC, Fitzke FW, Mollon JD, Moore AT. A detailed phenotypic study of "cone dystrophy with supernormal rod ERG". Br J Ophthalmol 2005; 89:332-9. [PMID: 15722315].
9. Robson AG, Webster AR, Michaelides M, Downes SM, Cowing JA, Hunt DM, Moore AT, Holder GE. "Cone Dystrophy with Supernormal Rod Electroretinogram": A Comprehensive Genotype/Phenotype Study Including Fundus Autofluorescence and Extensive Electrophysiology. Retina 2010; 30:51-62. [PMID: 19952985].
10. Sergouniotis PI, Holder GE, Robson AG, Michaelides M, Webster AR, Moore AT. High-resolution optical coherence tomography imaging in KCNV2 retinopathy. Br J Ophthalmol 2012; 96:213-7. [PMID: 21558291].
11. Vincent A, Robson AG, Holder GE. PATHOGNOMONIC (DIAGNOSTIC) ERGs A Review and Update. Retina 2013; 33:5-12. [PMID: 23263253].
12. Khan AO, Alrashed M, Alkuraya FS. 'Cone dystrophy with supranormal rod response' in children. Br J Ophthalmol 2012; 96:422-6. [PMID: 21900228].
13. Zobor D, Kohl S, Wissinger B, Zrenner E, Jagle H. Rod and Cone Function in Patients with KCNV2 Retinopathy. PLoS ONE 2012; 7:e46762-[PMID: 23077521].
14. Vincent A, Wright T, Garcia-Sanchez Y, Kisilak M, Campbell M, Westall C, Heon E. Phenotypic Characteristics including in vivo Cone Photoreceptor Mosaic in KCNV2-Related 'Cone Dystrophy with Supernormal Rod Electroretinogram'. Invest Ophthalmol Vis Sci 2013; 30:898-908. .
15. Tanimoto N, Usui T, Ichibe M, Takagi M, Hasegawa S, Abe H. PIII and derived PII analysis in a patient with retinal dysfunction with supernormal scotopic ERG. Doc Ophthalmol 2005; 110:219-26. [PMID: 16328930].
16. Wissinger B, Dangel S, Jagle H, Hansen L, Baumann B, Rudolph G, Wolf C, Bonin M, Koeppen K, Ladewig T, Kohl S, Zrenner E, Rosenberg T. Cone dystrophy with supernormal rod response is strictly associated with mutations in KCNV2. Invest Ophthalmol Vis Sci 2008; 49:751-7. [PMID: 18235024].
17. Friedburg C, Wissinger B, Schambeck M, Bonin M, Kohl S, Lorenz B. Long-term follow-up of the human phenotype in three siblings with cone dystrophy associated with a homozygous p.G461R mutation of KCNV2. Invest Ophthalmol Vis Sci 2011; 52:8621-9. [PMID: 21911584].
18. Wu H, Cowing JA, Michaelides M, Wilkie SE, Jeffery G, Jenkins SA, Mester V, Bird AC, Robson AG, Holder GE, Moore AT, Hunt DM, Webster AR. Mutations in the gene KCNV2 encoding a voltage-gated potassium channel subunit cause "cone dystrophy with supernormal rod electroretinogram" in humans. Am J Hum Genet 2006; 79:574-9. [PMID: 16909397].
19. Czirják G, Toth ZE, Enyedi P. Characterization of the heteromeric potassium channel formed by kv2.1 and the retinal subunit kv8.2 in Xenopus oocytes. J Neurophysiol 2007; 98:1213-22. [PMID: 17652418].
20. Hölter P, Kunst S, Wolloscheck T, Kelleher DK, Sticht C, Wolfrum U, Spessert R. The retinal clock drives the expression of Kcnv2, a channel essential for visual function and cone survival. Invest Ophthalmol Vis Sci 2012; 53:6947-54. [PMID: 22969075].
21. Beech DJ, Barnes S. Characterization of a voltage-gated K+ channel that accelerates the rod response to dim light. Neuron 1989; 3:573-81. [PMID: 2642011].
22. Thiagalingam S, McGee TL, Weleber RG, Sandberg MA, Trzupek KM, Berson EL, Dryja TP. Novel mutations in the KCNV2 gene in patients with cone dystrophy and a supernormal rod electroretinogram. Ophthalmic Genet 2007; 28:135-42. [PMID: 17896311].

23. Wissinger B, Schaich S, Baumann B, Bonin M, Jagle H, Friedburg C, Varsanyi B, Hoyng CB, Dollfus H, Heckenlively JR, Rosenberg T, Rudolph G, Kellner U, Salati R, Plomp A, De Baere E, Andrassi-Darida M, Sauer A, Wolf C, Zobor D, Bernd A, Leroy BP, Enyedi P, Cremers FP, Lorenz B, Zrenner E, Kohl S. Large deletions of the KCNV2 gene are common in patients with cone dystrophy with supernormal rod response. Hum Mutat 2011; 32:1398-406. [PMID: 21882291].

24. Nakamura N, Tsunoda K, Fujinami K, Shinoda K, Tomita K, Hatase T, Usui T, Akahori M, Iwata T, Miyake Y. Long-term Observation over Ten Years of Four Cases of Cone Dystrophy with Super-normal Rod Electroretinogram . Nippon Ganka Gakkai Zasshi 2013; In press.

25. Fujinami K, Tsunoda K, Hanazono G, Shinoda K, Ohde H, Miyake Y. Fundus autofluorescence in autosomal dominant occult macular dystrophy. Arch Ophthalmol 2011; 129:597-602. [PMID: 21555613].

26. Tsunoda K, Usui T, Hatase T, Yamai S, Fujinami K, Hanazono G, Shinoda K, Ohde H, Akahori M, Iwata T, Miyake Y. Clinical characteristics of occult macular dystrophy in family with mutation of Rplll gene. Retina 2012; 32:1135-47. [PMID: 22466457].

27. Marmor MF, Fulton AB, Holder GE, Miyake Y, Brigell M, Bach M. ISCEV Standard for full-field clinical electroretinography (2008 update). Doc Ophthalmol 2009; 118:69-77. [PMID: 19030905].

28. Ng PC, Henikoff S. SIFT: Predicting amino acid changes that affect protein function. Nucleic Acids Res 2003; 31:3812-4. [PMID: 12824425].

29. Adzhubei IA, Schmidt S, Peshkin L, Ramensky VE, Gerasimova A, Bork P, Kondrashov AS, Sunyaev SR. A method and server for predicting damaging missense mutations. Nat Methods 2010; 7:248-9. [PMID: 20354512].

30. Heginbotham L, Lu Z, Abramson T, MacKinnon R. Mutations in the K+ channel signature sequence. Biophys J 1994; 66:1061-7. [PMID: 8038378].

Articles are provided courtesy of Emory University and the Zhongshan Ophthalmic Center, Sun Yat-sen University, P.R. China. The print version of this article was created on 20 July 2013. This reflects all typographical corrections and errata to the article through that date. Details of any changes may be found in the online version of the article.

HMG Advance Access published May 21, 2013

Human Molecular Genetics, 2013 1–9
doi:10.1093/hmg/ddt210

Enhanced optineurin E50K–TBK1 interaction evokes protein insolubility and initiates familial primary open-angle glaucoma

Yuriko Minegishi[1], Daisuke Iejima[1], Hiroaki Kobayashi[1], Zai-Long Chi[1], Kazuhide Kawase[2], Tetsuya Yamamoto[2], Tomohisa Seki[3], Shinsuke Yuasa[3], Keiichi Fukuda[3] and Takeshi Iwata[1,*]

[1]Division of Molecular and Cellular Biology, National Institute of Sensory Organs, National Hospital Organization Tokyo Medical Center, Tokyo, Japan [2]Department of Ophthalmology, Gifu University School of Medicine, Gifu, Japan [3]Department of Cardiology, Keio University School of Medicine, Tokyo, Japan

Received March 13, 2013; Revised April 15, 2013; Accepted May 1, 2013

Glaucoma is the leading cause for blindness affecting 60 million people worldwide. The optineurin (OPTN) E50K mutation was first identified in familial primary open-angle glaucoma (POAG), the onset of which is not associated with intraocular pressure (IOP) elevation, and is classified as normal-tension glaucoma (NTG). Optineurin (OPTN) is a multifunctional protein and its mutations are associated with neurodegenerative diseases such as POAG and amyotrophic lateral sclerosis (ALS). We have previously described an E50K mutation-carrying transgenic (E50K^{tg}) mouse that exhibited glaucomatous phenotypes of decreased retinal ganglion cells (RGCs) and surrounding cell death at normal IOP. Further phenotypic analysis of these mice revealed persistent reactive gliosis and E50K mutant protein deposits in the outer plexiform layer (OPL). Over-expression of E50K in HEK293 cells indicated accumulation of insoluble OPTN in the endoplasmic reticulum (ER). This phenomenon was consistent with the results seen in neurons derived from induced pluripotent stem cells (iPSCs) from E50K mutation-carrying NTG patients. The E50K mutant strongly interacted with TANK-binding kinase 1 (TBK1), which prohibited the proper oligomerization and solubility of OPTN, both of which are important for OPTN intracellular transition. Treatment with a TBK1 inhibitor, BX795, abrogated the aberrant insolubility of the E50K mutant. Here, we delineated the intracellular dynamics of the endogenous E50K mutant protein for the first time and demonstrated how this mutation causes OPTN insolubility, in association with TBK1, to evoke POAG.

INTRODUCTION

Glaucoma is one of the world's leading cause of adult-onset blindness that causes optic nerve degeneration characterized by progressive and irreversible loss of retinal ganglion cells (RGCs) and retinal nerve fiber layer defects accompanied by the corresponding visual field damage (1). Open-angle glaucoma, the most prevalent subtype among various glaucomas, is further subdivided into two major types according to intraocular pressure (IOP). In the high-IOP type or primary open-angle glaucoma (POAG), elevated IOP due to disturbance of aqueous humor outflow in the trabecular meshwork or Schlemm's canal mechanically damages RGCs (2). In the normal-IOP type or normal-tension glaucoma (NTG), IOP elevation does not necessarily cause glaucoma, but some IOP-independent factors are thought to be involved (2). According to a population-based glaucoma survey conducted in Japan, NTG is the most prevalent subtype of glaucoma in the country (3, 4). This epidemiological study in Japan reported that the subjects' average IOP was ~15 mmHg and the POAG prevalence was almost equivalent in groups with IOP higher or lower than the average IOP (4). We have investigated the onset mechanism of the latter glaucoma subset, with lower IOP than average, as NTG. Interestingly enough, IOP-unrelated genetic mutations have been found recently in NTG (5, 6) and the Optineurin (OPTN) E50K mutation was the first one identified in familial NTG (7).

OPTN, a scaffold protein with various biological functions, has a few coiled-coil domains and a ubiquitin-binding domain

*To whom correspondence should be addressed at: Division of Molecular and Cellular Biology, National Institute of Sensory Organs, National Hospital Organization Tokyo Medical Center, 2-5-1 Higashigaoka, Meguro-ku, Tokyo 152-8902, Japan. Tel/Fax: +81 334111026; Email: iwatatakeshi@kankakuki.go.jp

OPTN E50K protein accumulates in the outer plexiform layer of the retinas of E50K^{tg} mice

Considering the previous report of the deposit-like pathology in motor neurons in the ALS-associated OPTN E478G mutation (20), we also investigated the localization of the OPTN E50K protein in the retinas of E50K^{tg} mice by immunohistochemistry. Negative control slides, treated with rabbit IgG cocktail alone, did not exhibit significant signals (Fig. 2A and B), while the retinas of E50K^{tg} mice exhibited positive staining for OPTN in the outer plexiform layer (OPL) and the inner nuclear layer (INL), as small dot-like deposits (Fig. 2D and F, arrows). The retinas of wild-type littermates did not exhibit such a pattern (Fig. 2C and E). We designed this transgenic mouse with N-terminally HA-tagged OPTN protein, which would enable us to confirm whether the deposits include E50K mutant protein. HA-tagged E50K was mainly detected in the OPL of the retinas in E50K^{tg} mice, which was consistent with the immunostaining results with the anti-OPTN antibody (Supplementary Material, Fig. S3D, arrows). Positive signals were not detected for OPTN in control slides in the retinas of wild-type mice and in those treated with the IgG alone (Supplementary Material, Fig. S3A–C). Thus, OPTN deposits in the retinas of E50K^{tg} mice were caused exclusively from the expression of the E50K mutant. These pathology findings point to the capacity of the E50K mutant protein to aggregate.

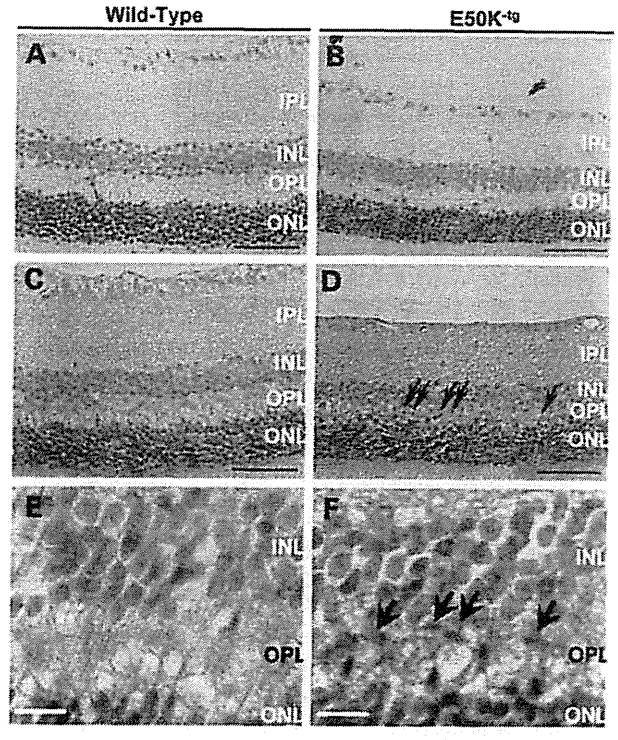

Figure 2. E50K mutant protein deposits in the retinas of E50K^{tg} mice. (**A**) Rabbit IgG negative control for the immunohistochemistry analysis of the retina of a wild-type mouse. (**B**) Rabbit IgG negative control for the immunohistochemistry analysis of the retina of an E50K^{tg} mouse. Both negative control slides showed minimum background staining. (**C**) Anti-OPTN immunohistochemistry of the wild-type mouse retina. Moderate OPTN signals were detected in luminal to inner layers of the retina. (**D**) Anti-OPTN immunohistochemistry of the E50K^{tg} mouse. In addition to the moderate OPTN signals similar to that in the wild-type mouse retina, some strong deposit-like signals from INL to OPL were detected (indicated with arrows). Scale bars = 50 μm. High magnification micrograph of the retina of (**E**) wild-type and (**F**) E50K^{tg} mice. Arrows indicate the OPTN deposit-like signals. Scale bars = 10 μm. The OPTN signals consists of, at least to some extent, the E50K^{tg} transgene product, from the results of immunohistochemistry analysis with an anti-HA antibody (Supplementary Material, Fig. S2D). INL, inner nuclear layer; OPL, outer plexiform layer; ONL, outer nuclear layer.

Examination of induced neural cells from NTG patient-derived iPSCs indicates disturbed OPTN transition from ER to Golgi and Golgi body constriction

To clarify the cause of E50K mutant protein deposits in the retinas of E50K^{tg} mice, we first examined the intracellular localization of wild-type OPTN and the E50K mutant by transfecting vectors encoding the two proteins fused with enhanced green fluorescent protein (EGFP) (^{EGFP}-OPTN and ^{EGFP}-E50K, respectively) into HEK 293 cells. ^{EGFP}-OPTN could be seen as small puncta widely distributed intracellularly, while ^{EGFP}-E50K was seen as larger puncta accumulated in the perinuclear region, and the Golgi body in the E50K-expressing cells was fragmented (Supplementary Material, Fig. S4B, arrowheads) as previously reported (10, 20). Since Golgi body formation and its membrane trafficking are associated with the endoplasmic reticulum (ER) (25, 26), ER structure was also examined using an ER detection kit (ER-ID, Enzo). Again, the wild-type OPTN was observed as small puncta dispersed within the cytosol (Fig. 3A), while the larger vesicles of the E50K mutant were accumulated in the perinuclear region surrounded by the ER membrane (Fig. 3B, arrows). To elucidate the intracellular localization of endogenous OPTN, we generated induced pluripotent stem cells (iPSCs) from peripheral blood mononuclear cells isolated from NTG patients with the mutation corresponding to E50K and examined OPTN localization in these cells. The pluripotency of iPSCs was confirmed by immunostaining with antibodies specific for Oct3 and Nanog, pluripotency markers (Supplementary Material, Fig. S5A). Neural induction was conducted as previously reported (27, 28) and neuronal differentiation was confirmed by staining with an antibody specific for Tuj1, a neuronal marker (Supplementary Material, Fig. S5B). iPSC-derived neural cells from NTG patients with the mutation corresponding to E50K were immunostained for OPTN and GM130, as a Golgi body marker, along with ER staining. In the iPSCs with wild-type OPTN, derived from a non-glaucoma subject, OPTN-associated vesicles were dispersed within the cells from ER to Golgi networks, in a pattern identical to that in HEK293 cells over-expressing wild-type OPTN (Fig. 3C). However, in the iPSCs from the NTG patient with the mutation corresponding to E50K, the number of OPTN-associated vesicles was decreased, compared with that in the control iPSCs, with dense aggregation in perinuclear regions and shrinkage of the ER/Golgi body (Fig. 3D). Upon microscopic examination under higher magnification, we found that wild-type OPTN frequently localized on the tips of Golgi ribbons (Fig. 3E), while the E50K OPTN mutant in iPSCs from NTG patients accumulated in the ER and Golgi body (Fig. 3F). Co-localization of wild-type OPTN and the Golgi body was

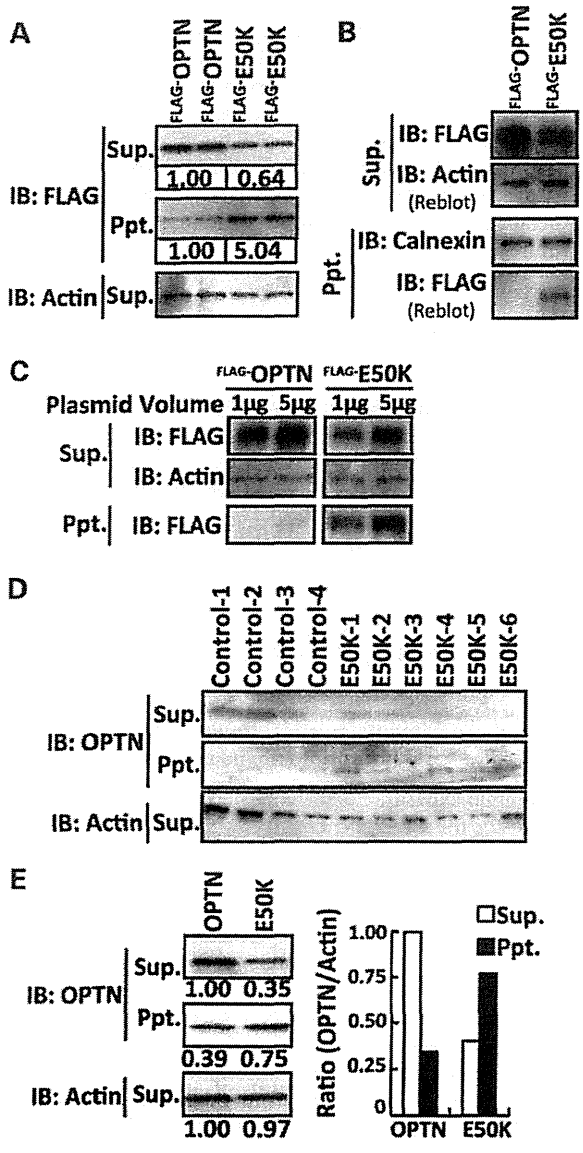

Figure 4. Distinct protein solubility of wild-type OPTN and the E50K mutant. (**A**) Wild-type OPTN and E50K expression under the same transfection condition. There were no differences in mRNA expressions under these transfection conditions (Supplementary Material, Fig. S4A). The 'Missing' E50K mutant protein was detected in the precipitated fraction (Ppt.), after supernatant (Sup.) collection. Semi-quantitative western blotting analysis was performed using Chemidoc (BioRad) with imaging software and the results are shown under each band. Approximately 2-fold reduction of E50K mutant protein in the Sup. fraction and 2- to 5-fold induction in the Ppt. fraction were observed. (**B**) Although calnexin, an ER membrane marker, is detected in both the Ppt. fraction of wild-type OPTN-expressing and E50K mutant-expressing cells, only the E50K mutant is detected in the Ppt. fraction. (**C**) The E50K mutant in the Ppt. fraction was increased in an E50K expression-dependent manner. (**D**) Endogenous expression and higher hydrophobicity of OPTN in iPSCs with the E50K mutation. Endogenous OPTN is also detected in the Ppt. fraction in iPSCs from E50K mutation-carrying NTG patients. (**E**) Abundant endogenous expression and higher hydrophobicity of OPTN in iPSC-derived neural cells 10 days after induction from E50K mutation-carrying NTG patients. Semi-quantitative western blotting analysis by Chemidoc with imaging software was performed and the results are shown under each band. The OPTN amounts in each fraction were normalized to the actin amount and then plotted. Sup., supernatant fraction; Ppt., precipitated fraction.

The enhanced affinity of TBK1 to the E50K mutant protein affects the proper oligomerization and solubility of OPTN

To elucidate the factors that affect the solubility of OPTN, we first examined the native state of wild-type OPTN and the E50K mutant. FLAG-tagged OPTN was expressed in cells and lysates were routinely prepared without detergent and separated by native-polyacrylamide gel electrophoresis (PAGE). Western blotting analysis after native-PAGE indicated more E50K-protein complexes compared with those formed by wild-type OPTN (Fig. 5A). The complexes were immunoprecipitated (IP) using an anti-FLAG antibody and then separated by SDS–PAGE, which revealed distinct binding partners of OPTN and E50K (Fig. 5B, OPTN, white arrowheads; E50K, black arrowheads). We identified each binding partner by liquid chromatography–tandem mass spectrometry (LC–MS/MS). The OPTN partner was identified as OPTN itself, indicating tight oligomerization, while the E50K protein partner was identified as TBK1, which has been previously shown to interact with OPTN by a yeast two-hybrid screening (31). Each candidate interacting partner was further confirmed by IP and western blotting (Fig. 5C and D). Intriguingly, E50K exhibited enhanced affinity to TBK1, while its self-oligomerization was largely decreased (Fig. 5C, arrowhead). Oligomerized OPTN bands clearly seen in wild-type OPTN were restored by treatment with intracellular degradation inhibitors (Supplementary Material, Fig. S7A, left panel, Oligomer lanes), indicating the importance of OPTN oligomerization in intracellular traffic and intracellular degradation. In contrast, these intracellular inhibitors had no effect on the diminished oligomerization of the E50K mutant (Supplementary Material, Fig. S7A right panel, Oligomer lanes). Treatment with a specific inhibitor treatment for TBK1, BX975 (32), was used to examine the relevance of TBK1 binding and the abnormal insolubility of the E50K mutant. BX795 treatment had no effects on the trace amounts of either wild-type OPTN (Supplementary Material, Fig. S7B) or calnexin in the Ppt. fraction (Fig. 5E); on the other hand, the amount of the insolubilized E50K mutant in the Ppt. fraction was drastically decreased by treatment with BX795 in a concentration-dependent manner. Prolonged BX795 treatment was able to restore the E50K mutant protein to the Sup. fraction (Fig. 5F). These findings indicate that the enhanced affinity of E50K for TBK1 is one of the initial pathogenic events that trigger the intracellular insolubility of OPTN leading to improper OPTN transition from the ER to the Golgi body.

DISCUSSION

The OPTN E50K mutation is the only mutation currently affirmed as causative for NTG, and therefore, it is a clinically relevant mutation for elucidating the mechanism of disease onset at a molecular level (4). Although the E50K mutation is a rare event in familial POAG, the pathology is usually progressive, leading to full blindness even under strict IOP control (Supplementary Material, Fig. S1) (17). Previous reports on E50K mutant phenotypes were focused mainly on *in vitro* models using over-expression studies. Though our initial report on the phenotypic analyses of E50K^{tg} mice was informative (19), there is a strong necessity for further establishment of the model for OPTN and its target molecules in the endogenous

Retinal vessel vulnerability in E50K^{-tg} mice is explained by these indirect extracellular E50K effects.

This study demonstrated that the E50K mutant is insoluble and is associated with the hydrophobic precipitate in lysates, compared with the wild-type OPTN, in iPSCs and iPSC-derived neural cells. Abnormal protein deposits, as shown in the retinas of the E50K^{-tg} mice, and protein hydrophobicity are frequently reported in neurodegenerative diseases (36–38). Recent reports in yeast models also supported the distinct hydrophobicities of wild-type OPTN and the E50K mutant (39). Although the prediction of isoelectric points (Compute pI/Mw, ExPASy) of wild-type OPTN and E50K do not differ (OPTN = 5.21, E50K = 5.26), their intracellular protein complex formation is considerably different. The amino acid characteristic of hydrophobic glutamate (E) against hydrophilic lysine (K) suggests that the E50K mutation is a possible charge swap mutation. E50K is located adjacent to the coiled-coil domain, which is a domain implicated in the interaction between OPTN and TBK1 (31, 15). The hydrophobicity of the E50K mutant was closely related with its enhanced interaction with TBK1, a well-known infection-responsive molecule. TBK1 induces macroautophagy by interacting with wild-type OPTN only under conditions of infection, and mediates crosstalk between innate immune response and autophagy (15). Additionally, the copy number variation of *TBK1* was associated with NTG onset (5, 6). The duplication of genes on chromosome 12q14 with familial POAG suggested that an extra copy of the *TBK1* gene and its copy number variation were responsible for NTG (40). More recently, NTG-related TBK1 mutations were also reported (41). Thus it is now well established that both *OPTN* and *TBK1* missense mutations are related with NTG onset. The abnormal physical protein interaction with TBK1 is responsible for the major cause of NTG in relation to the OPTN-E50K mutation. Together with the clinical facts, it has been reported that TBK1 has an important role in innate immunity pathways, and phosphorylated the ER-resident adaptor protein stimulator of IFN genes (STING) to enable IFN production (42, 43). Complexes of these molecules may be involved with the failure of the E50K OPTN protein to transition from ER to Golgi. Although TBK1 contributes to infection-related immunological responses, it also seems to contribute to the intracellular clearance of unnecessary components, such as by autophagy (15). Many other ophthalmic diseases, like macular diseases, are associated with abnormal protein metabolism (44); thus, the crosstalk of OPTN and TBK1 in the maintenance of intracellular clearance in retinal cells is likely to play a significant role in not only glaucomatous but also various other retinal diseases. Even though the exact function of TBK1 and the mechanism of the OPTN-TBK1 crosstalk in retinal homeostasis needs to be elucidated, compounds that abrogate the interaction between the E50K mutant and TBK1 are likely to be beneficial in the treatment of NTG patients.

Our current results pinpoint the molecular basis and concepts of NTG onset in E50K mutation-carrying patients and suggest that the RGC loss, the hallmark of glaucoma, is rather a terminal consequence of the sequential events, i.e. altered affinity of the E50K mutant inhibits self-oligomerization, leading to increased hydrophobicity, which affects downstream functions of OPTN, and eventually leads to cell death. Chronic and excessive accumulation of the E50K mutant protein recapitulated the partial neurodegenerative pathology, including reactive gliosis, vulnerability of retinal vessels and increased apoptotic cell death.

RGC loss is a hallmark of glaucoma; however, the results of this study showed that this phenomenon in E50K-NTG model is at the terminal stage of sequential abnormal events in the retina. In-depth characterization of the mutant protein in a physiologically relevant context and the proper choice/availability of a suitable animal model will help to elucidate and explore therapeutics for personalized treatment of glaucoma in the future.

MATERIALS AND METHODS

Antibodies and biochemical analysis

All the antibodies for biochemical studies were purchased from the following companies: anti-OPTN antibody (Cayman); anti-TBK1 antibody (Cell Signaling Technology); anti-FLAG (Sigma); anti-HA (Roche) and anti-Actin (Millipore). The TBK1 inhibitor, BX795, and cycloheximide were purchased from Calbiochem. Mini-PROTEAN TGX Gel and Transblot turbo system (BioRad) were used for native and SDS–PAGE western blotting according to the manufacturer's instructions. Quantitative western blotting was performed with ChemiDoc XRS+ with the Image lab software package (Biorad).

Animal experiments, preparation of retinal flat-mounts for staining and immunohistochemistry

All animal experiments were carried out in accordance with the Guide for the Care and Use of Laboratory Animals (National Institutes of Health) and the Association for Research in Vision and Ophthalmology Statement for the Use of Animals in Vision Research and approved by the Tokyo Medical Center Experimental Animal Committee. The OPTN mutant E50K^{-tg} mouse used in this study has been described previously (19). Twenty-two to 24-month-old male E50K^{-tg} mice ($n = 4$) and their littermates ($n = 4$) were sacrificed for the assessment of retinal gliosis. Both eyes were dissected and immunostained in flat-mounts as previously described (19). Briefly, dissected eyes were fixed in 2% paraformaldehyde and permeabilized with 0.1% Triton-phosphate-buffered saline (PBS). Non-specific binding was prevented by blocking with DAKO's serum-free blocking buffer, and all specimens were incubated with Alex488-conjugated anti-GFAP antibody (Millipore) for 4°C, over two nights. After radial dissection, retinas were mounted in DAKO's fluorescent mounting medium. A total of 16 retinal specimens, with four micrographs per one retinal specimen, were imaged by LSM700 confocal fluorescence microscopy (Zeiss) using a blinded method. Image analysis was conducted using the ZEN software (Zeiss) and the GFAP-positive area per retinal area was scored. The anti-OPTN (Cayman) and anti-HA (COVANCE) antibodies were used under heated antigen-retrieval conditions. Endogenous peroxidase was quenched by 3% H_2O_2 in MeOH. After primary antibody reaction for 4°C overnight, simple rabbit IgG-horse radish peroxidase (HRP) stain and mouse IgG-HRP stain for mouse tissue (Nichirei) were used as secondary HRP-conjugated polymers. After developing with 3,3′-diaminobenzidine (DAB) substrate, specimens were counter-stained with Gill's hematoxylin.

Phosphorylation of the autophagy receptor optineurin restricts Salmonella growth. *Science*, **333**, 228–233.
16. Ying, H. and Yue, B.Y. (2012) Cellular and molecular biology of optineurin. *Int. Rev. Cell. Mol. Biol.*, **294**, 223–258.
17. Aung, T., Rezaie, T., Okada, K., Viswanathan, A.C., Child, A.H., Brice, G., Bhattacharya, S.S., Lehmann, O.J., Sarfarazi, M. and Hitchings, R.A. (2005) Clinical features and course of patients with glaucoma with the E50K mutation in the optineurin gene. *Invest. Ophthalmol. Vis. Sci.*, **46**, 2816–2822.
18. Hauser, M.A., Sena, D.F., Flor, J., Walter, J., Auguste, J., Larocque-Abramson, K., Graham, F., Delbono, E., Haines, J.L., Pericak-Vance, M.A. *et al.* (2006) Distribution of optineurin sequence variations in an ethnically diverse population of low-tension glaucoma patients from the United States. *J. Glaucoma*, **15**, 358–363.
19. Chi, Z.L., Akahori, M., Obazawa, M., Minami, M., Noda, T., Nakaya, N., Tomarev, S., Kawase, K., Yamamoto, T., Noda, S. *et al.* (2010) Overexpression of optineurin E50K disrupts Rab8 interaction and leads to a progressive retinal degeneration in mice. *Hum. Mol. Genet.*, **19**, 2606–2615.
20. Maruyama, H., Morino, H., Ito, H., Izumi, Y., Kato, H., Watanabe, Y., Kinoshita, Y., Kamada, M., Nodera, H., Suzuki, H. *et al.* (2010) Mutations of optineurin in amyotrophic lateral sclerosis. *Nature*, **465**, 223–226.
21. Ganesh, B.S. and Chintala, S.K. (2011) Inhibition of reactive gliosis attenuates excitotoxicity-mediated death of retinal ganglion cells. *PLoS One*, **6**, e18305.
22. Wurm, A., Iandiev, I., Uhlmann, S., Wiedemann, P., Reichenbach, A., Bringmann, A. and Pannicke, T. (2011) Effects of ischemia-reperfusion on physiological properties of Muller glial cells in the porcine retina. *Invest. Ophthalmol. Vis. Sci.*, **52**, 3360–3367.
23. Giani, A., Thanos, A., Roh, M.I., Connolly, E., Trichonas, G., Kim, I., Gragoudas, E., Vavvas, D. and Miller, J.W. (2011) In vivo evaluation of laser-induced choroidal neovascularization using spectral-domain optical coherence tomography. *Invest. Ophthalmol. Vis. Sci.*, **52**, 3880–3887.
24. Ueda, K., Nakahara, T., Hoshino, M., Mori, A., Sakamoto, K. and Ishii, K. (2010) Retinal blood vessels are damaged in a rat model of NMDA-induced retinal degeneration. *Neurosci. Lett.*, **485**, 55–59.
25. Lasiecka, Z.M. and Winckler, B. (2011) Mechanisms of polarized membrane trafficking in neurons – focusing in on endosomes. *Mol. Cell. Neurosci.*, **48**, 278–287.
26. Farhan, H., Freissmuth, M. and Sitte, H.H. (2006) Oligomerization of neurotransmitter transporters: a ticket from the endoplasmic reticulum to the plasma membrane. *Handb. Exp. Pharmacol.*, **175**, 233–249.
27. Tsuji, O., Miura, K., Okada, Y., Fujiyoshi, K., Mukaino, M., Nagoshi, N., Kitamura, K., Kumagai, G., Nishino, M., Tomisato, S. *et al.* (2010) Therapeutic potential of appropriately evaluated safe-induced pluripotent stem cells for spinal cord injury. *Proc. Natl Acad. Sci. USA*, **107**, 12704–12709.
28. Tucker, B.A., Scheetz, T.E., Mullins, R.F., DeLuca, A.P., Hoffmann, J.M., Johnston, R.M., Jacobson, S.G., Sheffield, V.C. and Stone, E.M. (2011) Exome sequencing and analysis of induced pluripotent stem cells identify the cilia-related gene male germ cell-associated kinase (MAK) as a cause of retinitis pigmentosa. *Proc. Natl Acad. Sci. USA*, **108**, E569–576.
29. Sarfarazi, M. and Rezaie, T. (2003) Optineurin in primary open angle glaucoma. *Ophthalmol. Clin. North Am.*, **16**, 529–541.
30. Shen, X., Ying, H., Qiu, Y., Park, J.S., Shyam, R., Chi, Z.L., Iwata, T. and Yue, B.Y. (2011) Processing of optineurin in neuronal cells. *J. Biol. Chem.*, **286**, 3618–3629.
31. Morton, S., Hesson, L., Peggie, M. and Cohen, P. (2008) Enhanced binding of TBK1 by an optineurin mutant that causes a familial form of primary open angle glaucoma. *FEBS Lett.*, **582**, 997–1002.
32. Clark, K., Plater, L., Peggie, M. and Cohen, P. (2009) Use of the pharmacological inhibitor BX795 to study the regulation and physiological roles of TBK1 and IkappaB kinase epsilon: a distinct upstream kinase mediates Ser-172 phosphorylation and activation. *J. Biol. Chem.*, **284**, 14136–14146.
33. Ito, H., Nakamura, M., Komure, O., Ayaki, T., Wate, R., Maruyama, H., Nakamura, Y., Fujita, K., Kaneko, S., Okamoto, Y. *et al.* (2011) Clinicopathologic study on an ALS family with a heterozygous E478G optineurin mutation. *Acta Neuropathol.*, **122**, 223–229.
34. Imaizumi, Y., Okada, Y., Akamatsu, W., Koike, M., Kuzumaki, N., Hayakawa, H., Nihira, T., Kobayashi, T., Ohyama, M., Sato, S. *et al.* (2012) Mitochondrial dysfunction associated with increased oxidative stress and alpha-synuclein accumulation in PARK2 iPSC-derived neurons and postmortem brain tissue. *Mol. Brain*, **5**, 35.
35. Sippl, C., Bosserhoff, A.K., Fischer, D. and Tamm, E.R. (2011) Depletion of optineurin in RGC-5 cells derived from retinal neurons causes apoptosis and reduces the secretion of neurotrophins. *Exp. Eye Res.*, **93**, 669–680.
36. Nukina, N., Kosik, K.S. and Selkoe, D.J. (1987) Recognition of Alzheimer paired helical filaments by monoclonal neurofilament antibodies is due to crossreaction with tau protein. *Proc. Natl Acad. Sci. USA*, **84**, 3415–3419.
37. Hoffner, G., Kahlem, P. and Djian, P. (2002) Perinuclear localization of huntingtin as a consequence of its binding to microtubules through an interaction with beta-tubulin: relevance to Huntington's disease. *J. Cell Sci.*, **115**, 941–948.
38. LaVoie, M.J., Ostaszewski, B.L., Weihofen, A., Schlossmacher, M.G. and Selkoe, D.J. (2005) Dopamine covalently modifies and functionally inactivates parkin. *Nat. Med.*, **11**, 1214–1221.
39. Kryndushkin, D., Ihrke, G., Piermartiri, T.C. and Shewmaker, F. (2012) A yeast model of optineurin proteinopathy reveals a unique aggregation pattern associated with cellular toxicity. *Mol. Microbiol.*, **86**, 1531–1547.
40. Fingert, J.H., Darbro, B.W., Qian, Q., Van Rheeden, R., Miller, K., Riker, M., Solivan-Timpe, F., Roos, B.R., Robin, A.L. and Mullins, R.F. (2013) TBK1 and flanking genes in human retina. *Ophthalmic Genet.*, doi:10.3109/13816810.2013.768674.
41. Seo, S., Solivan-Timpe, F., Roos, B.R., Robin, A.L., Stone, E.M., Kwon, Y.H., Alward, W.L. and Fingert, J.H. (2013) Identification of proteins that interact with TANK binding kinase 1 and testing for mutations associated with glaucoma. *Curr. Eye Res.*, **38**, 310–315.
42. Saitoh, T., Fujita, N., Hayashi, T., Takahara, K., Satoh, T., Lee, H., Matsunaga, K., Kageyama, S., Omori, H., Noda, T. *et al.* (2009) Atg9a controls dsDNA-driven dynamic translocation of STING and the innate immune response. *Proc. Natl Acad. Sci. USA*, **106**, 20842–20846.
43. Tanaka, Y. and Chen, Z.J. (2012) STING specifies IRF3 phosphorylation by TBK1 in the cytosolic DNA signaling pathway. *Sci. Signal.*, **5**, ra20.
44. Shaw, P.X., Zhang, L., Zhang, M., Du, H., Zhao, L., Lee, C., Grob, S., Lim, S.L., Hughes, G., Lee, J. *et al.* (2012) Complement factor H genotypes impact risk of age-related macular degeneration by interaction with oxidized phospholipids. *Proc. Natl Acad. Sci. USA*, **109**, 13757–13762.
45. Mizushima, S. and Nagata, S. (1990) pEF-BOS, a powerful mammalian expression vector. *Nucleic Acids Res.*, **18**, 5322.
46. Seki, T., Yuasa, S., Oda, M., Egashira, T., Yae, K., Kusumoto, D., Nakata, H., Tohyama, S., Hashimoto, H., Kodaira, M. *et al.* (2010) Generation of induced pluripotent stem cells from human terminally differentiated circulating T cells. *Cell Stem Cell*, **7**, 11–14.

Doc Ophthalmol (2014) 128:219–228
DOI 10.1007/s10633-014-9436-z

CLINICAL CASE REPORT

Longitudinal clinical course of three Japanese patients with Leber congenital amaurosis/early-onset retinal dystrophy with *RDH12* mutation

Kazuki Kuniyoshi · Hiroyuki Sakuramoto · Kazutoshi Yoshitake · Kosuke Abe · Kazuho Ikeo · Masaaki Furuno · Kazushige Tsunoda · Shunji Kusaka · Yoshikazu Shimomura · Takeshi Iwata

Received: 11 February 2014 / Accepted: 10 April 2014 / Published online: 22 April 2014

Abstract
Purpose To report the longitudinal clinical course of three Japanese patients from two families with Leber congenital amaurosis/early-onset retinal dystrophy (LCA/EORD), and the results of next-generation DNA sequences on them.
Patients and methods The patients were three Japanese children: a 4-year-old girl, a 6-year-old boy, and a 3-year-old girl. Patients 1 and 2 were siblings, and patient 3 was from an unrelated family. Standard ophthalmic examinations including perimetry, electroretinography, optical coherence tomography, and ultrasonography were performed on each patient. The patients were observed for 28, 16, and 10 years. Whole exomes of the patients and their non-symptomatic parents were analyzed using a next-generation sequence technique.
Results The decimal visual acuity varied between 0.07 and 0.6 at the initial visit and decreased to counting finger to hand motion in their teens. Funduscopy showed diffuse retinal and macular degeneration. During the follow-up period, a posterior staphyloma developed and the macular area became atrophic. Patient 1 developed cataracts in her early twenties. Genetic analysis revealed a homozygous A126V substitution in the *RDH12* gene in all patients.
Conclusions The three patients with LCA/EORD had a progressive decrease of their vision with the formation of a posterior staphyloma. This is the first report of Japanese patients with LCA/EORD with a *RDH12* mutation.

A part of this paper was presented at the 8th congress of Asia Pacific Vitreo-retina Society in Nagoya, Japan, on December 7, 2013.

K. Kuniyoshi (✉) · H. Sakuramoto · K. Abe · Y. Shimomura
Department of Ophthalmology, Kinki University Faculty of Medicine, 377-2 Ohno-Higashi, Osaka-Sayama City, Osaka 589-8511, Japan
e-mail: kuniyoshi-kazuki@umin.net

K. Yoshitake · K. Ikeo
Laboratory of DNA Data Analysis, National Institute of Genetics, Shizuoka, Japan

M. Furuno
Transcriptome Technology Team, Life Science Accelerator Technology Group, Division of Genomic Technologies, RIKEN Center for Life Science Technologies, Yokohama, Japan

K. Tsunoda
Laboratory of Visual Physiology, National Institute of Sensory Organs, National Hospital Organization Tokyo Medical Center, Tokyo, Japan

S. Kusaka
Department of Ophthalmology, Sakai Hospital, Kinki University Faculty of Medicine, Sakai City, Osaka, Japan

T. Iwata
Division of Molecular and Cellular Biology, National Institute of Sensory Organs, National Hospital Organization Tokyo Medical Center, Tokyo, Japan

Keywords Leber congenital amaurosis · Early-onset retinal dystrophy · *RDH12* · Macular dystrophy · Posterior staphyloma · Electroretinogram · Next-generation sequence analysis

Introduction

Leber congenital amaurosis (LCA) is the most severe form of early-onset retinal dystrophy and was first reported by Theodor Leber in 1869 [1]. He reported blind infants who had nystagmus and no pupillary light reflexes, and their fundus was initially normal and progressed to pigmentary retinal dystrophy [1]. For the diagnosis of LCA, it is necessary to show the presence of searching nystagmus, absence of pupillary light reflexes, and non-recordable electroretinograms (ERGs) [2]. Leber also described milder forms of this disease [3], which is now referred to as early-onset severe retinal dystrophy (EOSRD), severe early-childhood-onset retinal dystrophy (SECORD), or early-onset retinal dystrophy (EORD). The appearance of the fundus of LCA/EORD varies widely, including normal fundus appearance, flecked retina, diffuse pigmentary retinal degeneration, and macular coloboma/posterior staphyloma. In addition, keratoconus and cataract can be present in these patients [4].

Most cases of LCA/EORD have an autosomal recessive inheritance pattern. To date, 17 causative genes have been identified for LCA/EORD (LCA1-17, Table 1) [5, 6]. Since *RDH12* was reported as a causative gene for LCA/EORD in 2004 [7, 8], several studies have reported on the phenotype of LCA/EORD patients with a *RDH12* mutation [9–16]. These studies reported a progressive reduction in vision leading to legal blindness in young adulthood, and the presence of diffuse retinal degeneration with macular degeneration and cataract formation [7–16]. However, the longitudinal clinical course of cases of LCA/EORD with the *RDH12* mutation has not been reported.

Table 1 Genes reported as causative for Leber congenital amaurosis or early-onset retinal dystrophy (LCA/EORD) [5,6]

Phenotype	Name	Loci	Year reported in LCA/EORD	Note
LCA1 (ar)	*GUCY2D*	17q13.1	1996	CORD6 (ad)
LCA2 (ar)	*RPE65*	1q31.3-2	1997	keratoconus, RP20 (ar)
LCA3 (ar)	*SPATA7*	14q31.3	2009	
LCA4 (ar)	*AIPL1*	17p13.2	2000	macular degeneration, juvenile CRD (ad)
LCA5 (ar)	*LCA5*	6q14.1	2003	coloboma
LCA6 (ar)	*RPGRIP1*	14q11.2	2001	CORD13 (ar)
LCA7 (ad/ar)	*CRX*	19q13.32	1998	coloboma, CORD2 (ad)
LCA8 (ar)	*CRB1*	1q31.3	2001	coloboma, PPRPE (ar), RP12 (ar)
LCA9 (ar)	*NMNAT1*	1q36.22	2012	coloboma
LCA10 (ar)	*CEP290*	12q21.32	2006	BBS14 (ar), JBTS5 (ar), SLSN6 (ar), MKS4 (ar)
LCA11 (ad)	*IMPDH1*	7q32.1	2006	RP10 (ad)
LCA12 (ar)	*RD3*	1q32.3	2006	
LCA13 (ar)	*RDH12*	14q24.1	2004	maculopathy, RP53 (ad)
LCA14 (ar)	*LRAT*	4q32.1	2001	
LCA15 (ar)	*TULP1*	6q21.31	2004	maculopathy, RP14 (ar)
LCA16 (ar)	*KCNJ13*	2q37.1	2011	SVD (ad)
LCA17 (ar)	*GDF6*	8q22.1	2013	

ar autosomal recessive, *ad* autosomal dominant, *CORD* and *CRD* cone-rod dystrophy, *RP* retinitis pigmentosa, *PPRPE* RP with parafoveolar preservation of the retinal pigment epithelium, *BBS* Bardet-Biedl syndrome, *JBTS* Joubert syndrome, *SLSN* Senior-Loken syndrome, *MKS* Meckel syndrome, *SVD* snowflake vitreoretinal degeneration

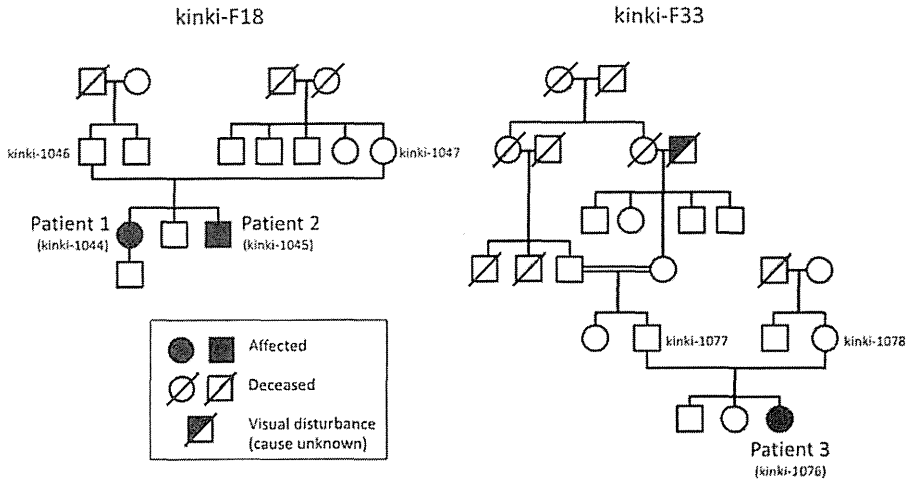

Fig. 1 Pedigrees of two unrelated families with Leber congenital amaurosis/early-onset retinal dystrophy (LCD/EORD) with *RDH12* mutation. Patients 1 and 2 were siblings (*left*, kinki-F18), and Patient 3 is from an unrelated family (*right*, kinki-F33). No consanguinity was reported between parents of the patients

We report the 10- to 28-year continuous course of three Japanese patients with LCA/EORD, and the results of next-generation sequence analyses on them.

Patients and methods

The patients were three Japanese individuals from two unrelated families (Fig. 1). Patients 1 and 2 were siblings (kinki-F18), and Patient 3 was a member of another unrelated family (kinki-F33; Fig. 1).

The research protocol was approved by the Ethics Review Board of the Kinki University Faculty of Medicine in November 2011, and the procedures conformed to the tenets of the Declaration of Helsinki. The genetic analysis was performed after obtaining a signed informed consent form from all patients and/or their parents.

Clinical studies

The ophthalmic examinations consisted of measurements of the visual acuity, slit-lamp biomicroscopy, ophthalmoscopy, Goldmann kinetic perimetry, full-field ERGs, optical coherence tomography (OCT), and ultrasonography. ERG recordings were performed according to the guideline of the International Society for Clinical Electrophysiology of Vision (ISCEV Standard, 2008 update) [17]. OCT was performed with the Cirrus™ HD-OCT version 5.1 (Carl Zeiss Meditec, Dublin, CA, USA). All clinical tests were performed in the Kinki University Hospital, and all patients were examined yearly from the initial visit to year 2013.

DNA preparation and exome sequencing analysis

The genetic analyses were performed in 2013. We obtained venous blood samples from the patients and their non-symptomatic parents in the Kinki University Hospital. The blood samples were sent to the Division of Molecular and Cellular Biology in National Institute of Sensory Organs of the National Hospital Organization Tokyo Medical Center, and genomic DNA was extracted from the blood samples using Gentra Puregene Blood Kit (Qiagen, Tokyo, Japan). The purified genomic DNA was sent to RIKEN or Macrogen Japan (Tokyo, Japan) and shared with Covaris Ultrasonicator™ (Covaris, Woburn, MA, USA). Construction of paired-end sequence libraries and exome capture were performed using the Agilent Bravo Automated Liquid Handling Platform with SureSelect XT Human All Exon V4 + UTRs kit (Agilent Technologies, Santa Clara, CA, USA) according to the manufacturer's instructions. Enriched libraries were sequenced with the Illumina HiSeq 2000 sequencer (San Diego, CA, USA), according to the manufacturer's instructions for 100-bp paired-end sequencing. The results of the sequence analysis were sent to Laboratory of DNA Data Analysis in National Institute of Genetics and analyzed. Reads were mapped to the reference human genome (1,000 genomes, phase 2 reference, hs37d5) with the Burrows-Wheeler Aligner software, version 0.6.2 [18]. Duplicated reads were then removed by Picard MarkDuplicates module version 1.62, and mapped reads around insertion–deletion polymorphisms (INDELs) were realigned using the Genome Analysis

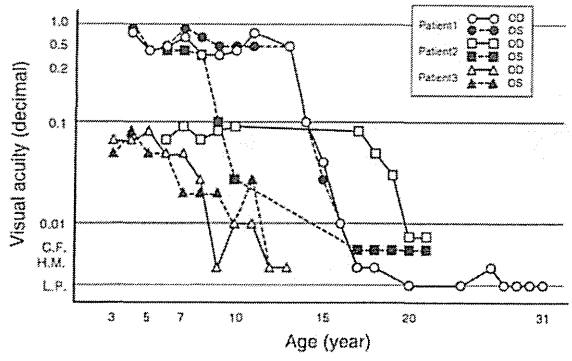

Fig. 2 Clinical course of visual acuity in each patient. *OD* oculus dexter, *OS* oculus sinister

Toolkit (GATK) version 2.7-4 [19]. Base-quality scores were recalibrated using GATK. The calling of mutations was performed using the GATK UnifiedGenotyper module, and the called single-nucleotide variants and INDELs were annotated with the snpEff software, version 3.3 [20]. The mutations were annotated with the snpEff score ("HIGH," "MODERATE," or "LOW") and with the allele frequency in the 1,000 genomes database and Human Genetic Variation Browser (HGVD) [21]. The mutations were then filtered so that only those with "HIGH" or "MODERATE" snpEff scores indicating that the amino acid sequence would be functionally affected, and a frequency <1 % in the 1,000 genomes database and HGVD were further analyzed. We also used new variations, which were not found in the in-house database of exome data of seven people with control individuals without ocular diseases. Mutations were classified by hereditary information into homozygous recessive, heterozygous recessive, and de novo mutations in the family members. Filtered mutations were scored with PolyPhen software version 2.2.2 [22], which predicts the effect on the structure and function of the protein. This exome analysis pipeline is available at Management and Analysis System for Enormous Reads (Maser) [23].

Results

The clinical course of the visual acuity in the three patients is presented in Fig. 2. Summaries of the clinical findings are shown in Figs. 3, 4, and 5.

Patient 1 (Fig. 3, kinki-1044 in Fig. 1): Patient 1 was a girl who was 4-year old when we first examined her in 1986. Her parents reported that she seemed to have difficulty in the dark from the age of 3 years. Her decimal best-corrected visual acuity (BCVA) at the initial visit was 0.6 with +1.25 diopter sphere (DS) and −0.75 D cylinder (DC) ax 160° in the right eye and 0.6 with +0.5 DS and −0.25 DC ax 20° in the left eye. Her visual fields were severely constricted, and ophthalmoscopy showed diffuse retinal degeneration with macular degeneration (Fig. 3). Her fundi appeared reticulated before the age 10 years. Her vision markedly decreased in her middle teens resulting in hand motion vision at age 17 years (Fig. 2). At this age, the macular degeneration appeared atrophic and a posterior staphyloma was present in both eyes (Fig. 3). A posterior subcapsular cataract was noticed when she was 23-year old. She is now 31-year old, and her vision is light perception in both eyes (Fig. 2).

Fig. 3 Fundus photographs (*left*), optical coherence tomographic (OCT) and ultrasonographic images (*lower left*), Goldmann kinetic visual fields (*right*), and full-field ERGs (*bottom right*) of Patient 1. Fundus photographs and OCT images taken at age 27 and 30 years are blurred because of cataracts. The last perimetric examination was performed on August 12, 1999, when no isopter could not be detected. The flash ERGs are dark-adapted 30.0 ERG with 20-J xenon strobe, and the flicker ERG was recorded using red light-emitting diode built-in contact lens electrode (Tomey, Nagoya, Japan)

Single-bright flash full-field ERGs recorded at age 9 years were non-recordable, and the flicker ERGs were barely recordable (Fig. 3). OCT and ultrasonography performed at 30 and 31 years of age showed deep excavation and a thinning of the retina at the posterior pole of both eyes (Fig. 3). The axial length at age 31 years was 22.72 ± 0.05 mm in the right eye and 21.20 ± 0.09 mm in the left eye.

When the sequences of her whole exome were compared with the reference human genome (hs37d5), 940,138 mutations were found. We focused only on mutations that could change the amino-acid sequence and excluded common mutations by 1,000 genomes, HGVD [21], and our in-house database (see methods). As a result, 467 mutations remained as candidate mutations. We filtered the remaining mutations by using the pattern of inheritance (homozygous recessive, heterozygous recessive, or de novo mutation) with her parents and her brother (Patient 2) and found only 2 genes as causal candidates. Finally, *RDH12*, which was the only one of the genes registered in the RetNet database of genes and the loci causing inherited retinal diseases [6], was assumed to be the

OD OS

31st October, 1986 (at age 4 years 8 months)

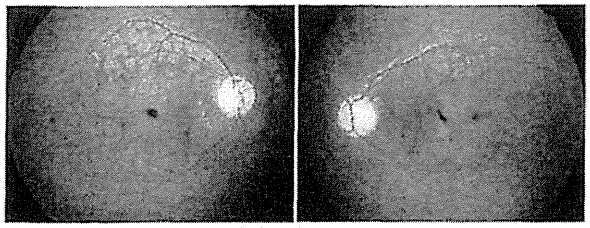

16th August, 1991 (at age 9 years 5 months)

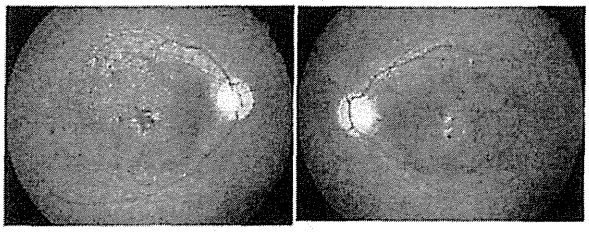

12th August, 1999 (at age 17 years 5 months)

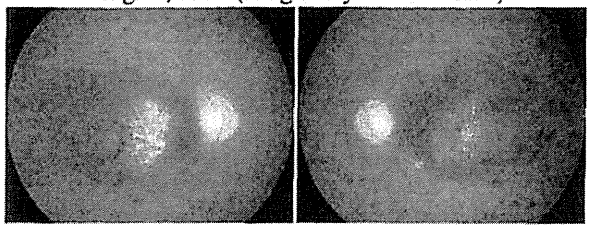

4th March, 2009 (at age 27 years)

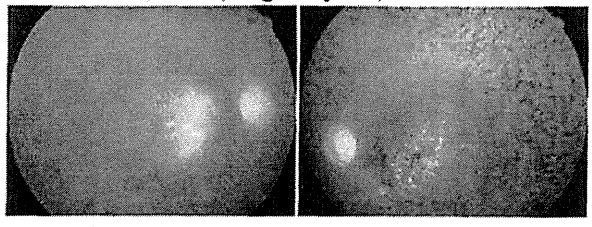

24th September, 2012 (at age 30 years)

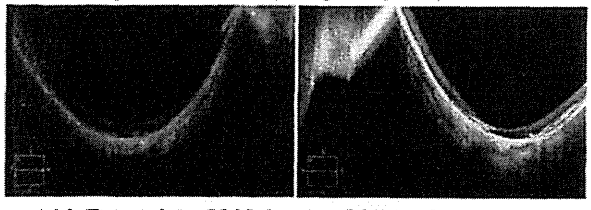

14th December, 2013 (at age 31 years)

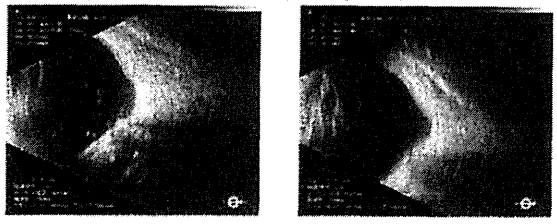

OS OD

31st October, 1986 (at age 4 years 8 months)

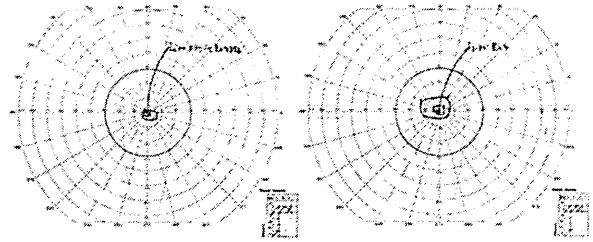

7th January, 1992 (at age 9 years 10 months)

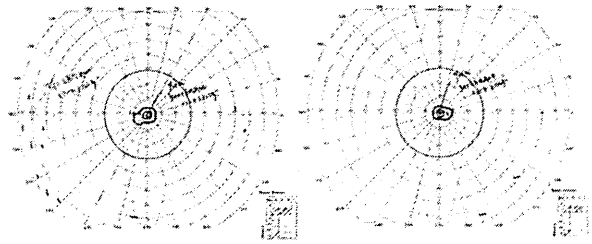

12th August, 1999 (at age 17 years 5 months)

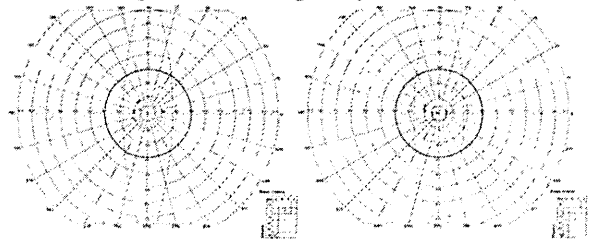

16th August, 1991 (at age 9 years 5 months)

Flash ERG Flicker ERG

OD
OS

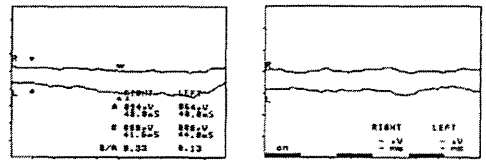

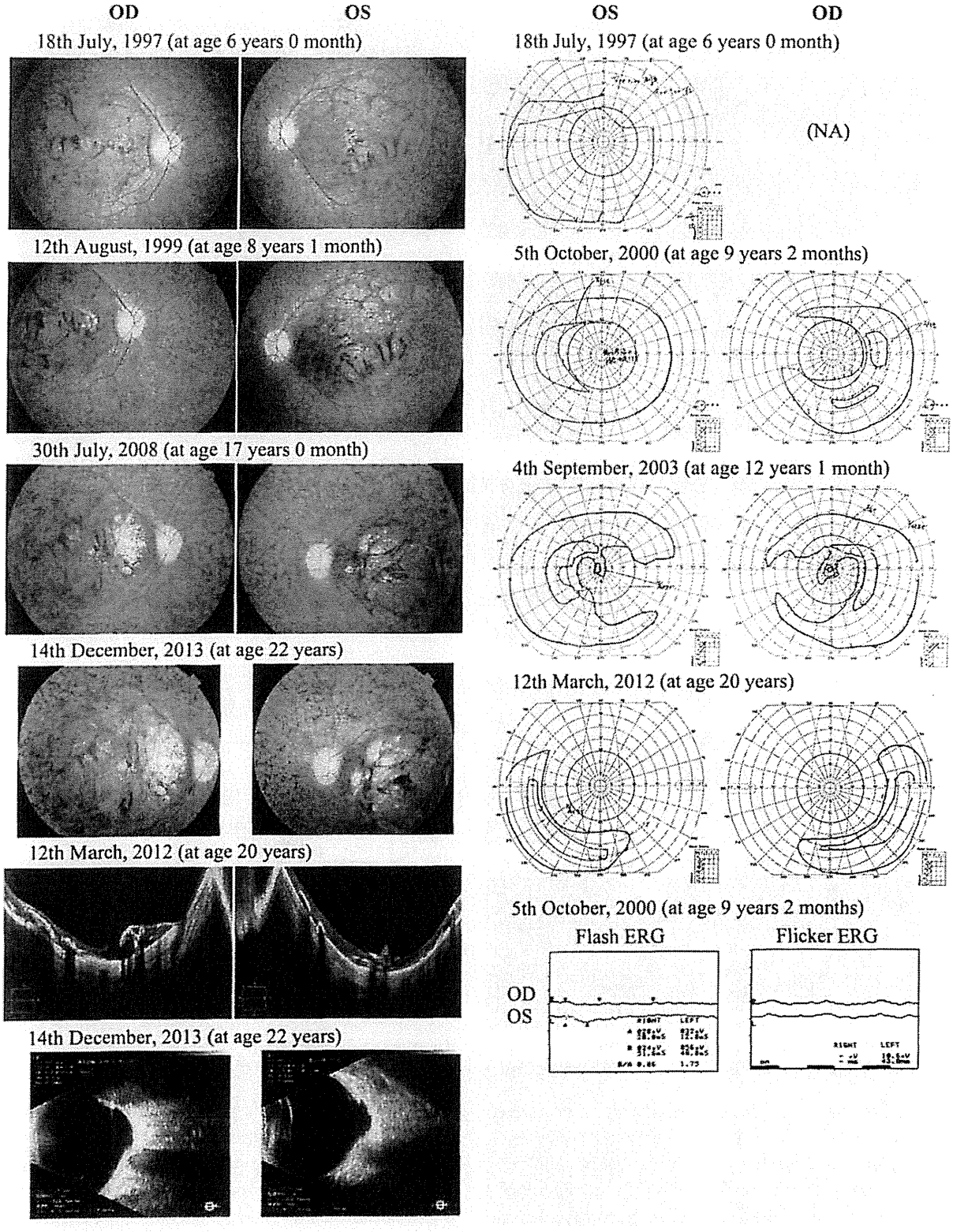

Fig. 4 Fundus photographs (*left*), OCT and ultrasonographic images (*lower left*), Goldmann kinetic visual fields (*right*), and full-field ERGs (*bottom right*) of Patient 2. Patient 2 was younger brother of Patient 1 (Figs. 1, 3). *NA* not available

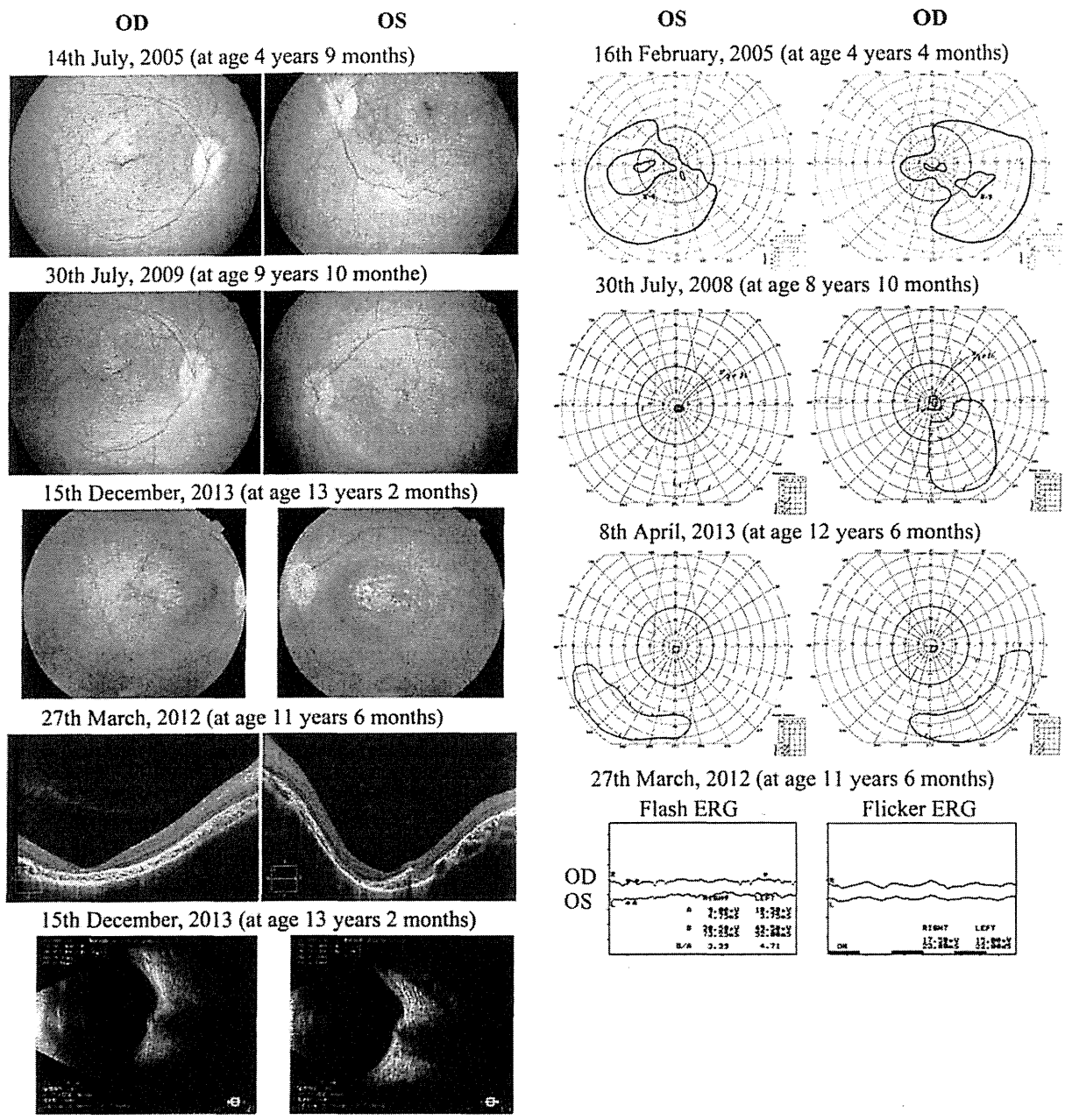

Fig. 5 Fundus photographs (*left*), OCT and ultrasonographic images (*lower left*), Goldmann kinetic visual fields (*right*), and full-field ERGs (*bottom right*) of Patient 3. Patient 3 was from unrelated family to that of Patients 1 and 2 (Fig. 1)

disease-causing gene. Then, genetic analysis revealed a homozygous c.377C>T transition in exon 4 resulting in an alanine126 to valine substitution (A126V) in the *RDH12* gene. Genetic analyses of her non-symptomatic parents (kinki-1046 and 1047, Fig. 1) revealed a heterozygous A126V substitution in the *RDH12* gene.

Patient 2 (Fig. 4, kinki-1045 in Fig. 1): Patient 2 was a boy who was 6-year old when we first examined him in 1997. He was the younger brother of Patient 1 (Fig. 1). He visited our clinic because his parents noticed he was having visual difficulties since age 5 years. His decimal visual acuity was 0.07 in his right eye. The vision was uncorrectable, and his left BCVA was 0.4 with 0 DS and −1.5 DC ax 160°. Ophthalmoscopy showed diffuse retinal degeneration, but it was especially severe in the macula which was similar

to that of his older sister, Patient 1 (Fig. 3, 4). The fundi appeared reticulated before the age 10 years. The macular degeneration gradually spread, and a posterior staphyloma developed and progressed in both eyes (Fig. 4). His central vision decreased to hand motion in his late teens (Fig. 2). He is now 22-year old, and he still has some peripheral vision but no cataracts in both eyes.

The full-field ERGs, OCT, and ultrasonographic findings were similar to those of his older sister (Patient 1), namely, non-recordable single-bright flash ERGs, barely recordable flicker ERGs, and deep excavation and thin retina at the posterior pole of both eyes (Fig. 4). The axial length at age 22 years was 23.82 ± 0.05 mm in the right eye and 24.06 ± 0.02 mm in the left eye.

Genetic analysis revealed a homozygous A126V substitution in *RDH12* gene, the same as his sister (Patient 1).

Patient 3 (Fig. 5, kinki-1076 in Fig. 1): Patient 3 was a girl who was 3-year old when we first examined her in 2004. She was a member of a family (kinki-F33) unrelated to that of Patients 1 and 2 (Fig. 1). She was brought to our clinic because of esotropia and nystagmus. Her decimal BCVA was 0.07 with +6.0 DS and −1.0 DC ax 115° in the right eye and 0.07 with +5.5 DS and −1.5 DC ax 175° in the left eye. Ophthalmoscopy showed diffuse retinal degeneration with pigmentation in the macular area (Fig. 5). Her fundi appeared reticulated before the age 10 years. She was followed until the age of 13 years, and her vision gradually decreased to light perception in both eyes (Fig. 2).

Single-bright flash full-field ERGs were non-recordable, and flicker ERGs were barely recordable at age 11 years (Fig. 5). OCT and ultrasonography performed at 11 and 13 years of age revealed excavation of the posterior pole of both eyes (Fig. 5). The axial length at age 13 years was 20.92 ± 0.37 mm in the right eye and 21.22 ± 0.93 mm in the left eye.

When the sequence of her whole exome was compared with the reference human genome (hs37d5), 1,488,313 mutations were found. After excluding common mutations, 406 mutations remained. We filtered the remaining mutations by the pattern of inheritance with her parents and found 16 genes as causal candidates. Finally, they were compared to that of Patients 1 and 2, and only *RDH12* was shared between three patients. As a result, genetic analysis showed a homozygous c.377C>T transition in exon 4 resulting in alanine126 to valine substitution (A126V) in the *RDH12* gene. Genetic analyses on her non-symptomatic parents (kinki-1077 & 1078, Fig. 1) showed heterozygous A126V substitution in the *RDH12* gene.

Discussion

ERG findings in carrier relatives

The *RDH12* gene is located at 14q 24.1 and encodes a photoreceptor cell retinol dehydrogenase. Mutation of the *RDH12* gene is estimated to account for <4 % of all autosomal recessive LCA/EORD patients [5, 8]. To date, 16 different mutations have been reported in this gene [6]; however, the homozygous substitution of A126V in the *RDH12* gene has never been reported except in a highly consanguineous Arabic family [13] and our patients. In the Arabic family, a non-symptomatic relative who was a heterozygous carrier of A126V had markedly reduced rod ERGs, and the cone ERGs were at the lower limits of normal [13]. Another study reported that heterozygous mutations in the *RDH12* gene can cause a late-onset, relatively mild autosomal dominant retinitis pigmentosa [24].

The parents of our patients were non-symptomatic, and their fundi were normal. The rod and cone ERGs performed on three of them (kinki-1047, kinki-1077, and kinki-1078 in Fig. 1) were normal.

Clinical course of visual acuity

The initial visual disturbance in our patients was noticed at age 2–5 years, and there was a progressive decrease thereafter (Fig. 2). Their central vision decreased to light perception in the teens. Patients 2 and 3 maintained some peripheral vision at age 22 and 13 years although Patient 1 lost vision in the entire visual field at age 17 years (Figs. 3, 4, 5).

The vision in patients with LCA/EORD was investigated by Fulton et al. [25] and Walia et al. [26]. Walia et al. [26] related the vision of patients with LCA/EORD to their causative genes and reported that LCA/EORD caused by *RPE65* (LCA2), *CRB1* (LCA8), and *RDH12* (LCA13) mutations led to a wide variations in visual disturbances, whereas LCA/EORD caused by *GUCY2D* (LCA1), *AIPL1* (LCA4), *RPGRIP1* (LCA6), and *CRX* (LCA7) gene mutations had severe visual disturbances which began in the first year of life. Other studies on LCA/EORD associated

with *RDH12* mutations reported an initial vision reduction occurring between birth to 20 years with most of them at age 3–7 years [7–16].

These results are consistent with our patients who had decreased vision at age 2–5 years and loss of their central vision in their teens (Fig. 2).

Coloboma/posterior staphyloma and LCA/EORD

The fundus of our three patients appeared similar; namely, they showed diffuse retinal degeneration and macular atrophy (Figs. 3, 4, 5). The fundi also had a reticulated appearance (Figs. 3, 4, 5). These findings are similar to the phenotype reported for *RDH12*-associated LCA/EORD [7–16].

In our patients, the macular degeneration progressed to atrophic macula with the formation of a posterior staphyloma which resembled a coloboma (Figs. 3, 4, 5). The relationships between LCA and macular coloboma have been discussed in several papers [27–29], before the causative genes for LCA/EORD were discovered. Recently, a macular coloboma/posterior staphyloma was reported in patients with *LCA5* (LCA5) [30], *CRX* (LCA7) [31], *CRB1* (LCA8) [32], *NMNAT1* (LCA9) [33], and *RDH12* (LCA13) mutations [7, 9–11, 14, 16]. A relationship between LCA/EORD and the macular coloboma/posterior staphyloma is still unknown. Single-gene mutation cannot explain the formation of a macular coloboma/posterior staphyloma because they are present in cases of LCA/EORD associated with several different causative genes.

In our patients, the reticulated appearance of the fundus was present in early childhood, and it became less apparent after the formation of the posterior staphyloma. Whether the reticulated appearance was related to the development of the staphyloma was not determined.

One limitation of this study is the small number of the patients. In addition, a more detailed screened investigation of the phenotypes and genotypes of patients with LCA/EORD is needed to confirm our results.

In conclusion, we report the longitudinal clinical course of three patients in two families with LCA/EORD who had homozygous A126V substitution in the *RDH12* gene. All of the patients had a progressive retinal degeneration and posterior staphyloma, and impairment of the central vision. This is the first report of Japanese patients with LCA/EORD which was caused by *RDH12* gene mutation.

Acknowledgments Authors express gratitude to Professor Toshifumi Otori, M.D., who transferred the longitudinal clinical data to us and gave us suggestive advice on this study. The authors wish to acknowledge RIKEN GeNAS for the sequencing of the Exome enriched libraries. This research was supported by the research grants to T.I. and K.K. from the Ministry of Health, Labour and Welfare, Japan (13803661), to K.T. and K.K. from the Ministry of Health, Labour and Welfare, Japan (23164001), Y.S from the Ministry of Health, Labour and Welfare, Japan (82259921), S.K. and K.K. from Japan Society for the Promotion of Science, Japan (23592597), and to M.F. from the Japanese Ministry of Education, Culture, Sports, Science and Technology (MEXT) for RIKEN Omics Science Center.

Conflict of interest All authors have no commercial interests related to this research.

References

1. Leber T (1869) Ueber Retinitis pigmentosa und angeborene Amaurose. Graefes Arch Klin Exp Ophthalmol 15:1–25
2. Franceschetti A, Dieterlé P (1954) Importance diagnostique et pronostique de l' électrorétinogramme (ERG) dans les dégénérescences tapéto-rétiniennes avec rétrécissement du champ visuel et héméralopie. Confin Neurol 14:184–186
3. Leber T (1916) Die Pigmentdegeneration der Netzhaut und die mit ihr verwandten Erkrankungen. In: Saemisch T, Elschnig A (eds) Graefe-Saemisch-Hess Handbuch der gesamten Augenheilkunde. Zweite Hälfte. Verlag von Wilherm Engelmann, Leipzig, pp 1076–1225
4. Weleber RG & Gregory-Evans K (2006) Leber congenital amaurosis. In: Hinton DR (ed), Ryan SJ (ed in chief) Retina, 4th edn, vol 1. Elsevier Inc., Philadelphia, pp 455–457
5. Weleber RG, Francis PJ, Trzupek KM & Beattie C (2014) Leber congenital amaurosis. In: Pagon RA (ed in chief), Adam MP, Bird TD, Dolan CR, Fong CT, Smith RJH, Stephens K (eds) GeneReviews™. NCBI Bookshelf. http://www.ncbi.nlm.nih.gov/books/NBK1298/. Accessed 12 Mar 2014
6. Daiger SP, The University of Texas Health Science Center (2014) RetNet™. Retinal information network. Updated 10 Mar 2014. https://sph.uth.edu/retnet. Accessed 12 March 2014
7. Jenecke AR, Thompson DA, Utermann G, Becker C, Hübner CA, Schmid E, McHenry CL, Nair AR, Rüschendorf F, Heckenlively J, Wissinger B, Nürnberg P, Gal A (2004) Mutations in *RDH12* encoding a photoreceptor cell retinol dehydrogenase cause childhood-onset severe retinal dystrophy. Nat Genet 36:850–854
8. Perrault I, Hanein S, Gerber S, Barbet F, Ducroq D, Dollfus H, Hamel C, Dufier JL, Munnich A, Kaplan J, Rozet JM (2004) Retinal dehydrogenase 12 (*RDH12*) mutations in Leber congenital amaurosis. Am J Hum Genet 75:639–646
9. Jacobson SG, Cideciyan AV, Aleman TS, Sumaroka A, Schwartz SB, Windsor EAM, Roman AJ, Heon E, Stone EM, Thompson DA (2007) *RDH12* and *RPE65*, visual cycle genes causing Leber congenital amaurosis, differ in disease expression. Invest Ophthalmol Vis Sci 48:332–338